Rational design of selective bispecific EPO-R/CD131 agonists

Kailyn E. Doiron[1,2,3], Jeffrey C. Way[1,2], Pamela A. Silver[1,2]*

1. Department of Systems Biology, Harvard Medical School, Boston, Massachusetts, 02115, USA
2. Wyss Institute for Biologically Inspired Engineering, Harvard University, Boston, Massachusetts 02115, USA
3. Harvard Systems, Synthetic and Quantitative Biology PhD Program, Harvard University, Cambridge, Massachusetts 02138

Corresponding author: Jeffrey C. Way
jeffrey_way@hms.harvard.edu

Abstract

Erythropoietin (EPO) suppresses apoptosis and promotes survival by signaling through EPO-R/EPO-R on hematopoietic progenitors or EPO-R/CD131 on non-hematopoietic cells. However, EPO signaling through EPO-R/CD131 is controversial and there is no solved structure of a complex. Here, we constructed a structural model of EPO-R/CD131 and designed several anti-EPO-R, anti-CD131 bispecific proteins that selectively activate EPO-R/CD131. Treatment with these fusion proteins is sufficient to activate STAT5 phosphorylation downstream of EPO-R/CD131 without engaging EPO-R/EPO-R. We demonstrated that proteins with a tandem scFv or bispecific antibody format activate EPO-R/CD131, in contrast to an equimolar mixture of the individual scFvs. Finally, we explored the effect of modifications to binding domain arrangement and linker length and found results consistent with our structural model of an EPO-R/CD131 complex. These findings highlight the utility of bispecific scaffolds in the development of cytokine receptor agonists and provide a foundation for the study of EPO-R/CD131 biology and future clinical development.

Graphical Abstract

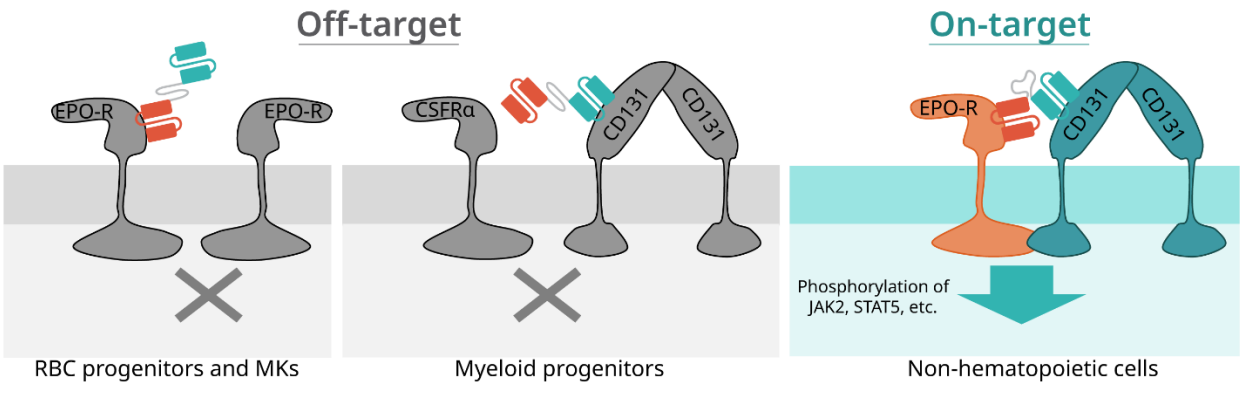

Introduction

Erythropoietin (EPO) is a cytokine that is essential for red blood cell (RBC) maturation. EPO promotes erythropoiesis by suppressing apoptosis in a subset of erythroid progenitors, enabling their survival and subsequent differentiation (Watowich, 2011). EPO signaling in these cells is well-characterized and begins through binding of EPO to the homodimeric EPO receptor (EPO-R/EPO-R) (Broudy *et al.*, 1991; Philo *et al.*, 1996; Watowich, 1999). Ligand binding induces structural changes in the cytoplasmic domains of EPO-R, triggering transactivation of JAK2 and then STAT5 (Witthuhn *et al.*, 1993; Chin *et al.*, 1996; Klingmüller *et al.*, 1996). Once STAT5 is phosphorylated by JAK2, it translocates to the nucleus where it activates expression of genes necessary for the survival, proliferation and differentiation of erythroid cells, including the anti-apoptotic proteins Bcl-2, Bcl-XL (Wojchowski *et al.*, 1999; Watowich, 2011). Due to its ability to promote erythropoiesis, EPO and its derivatives (e.g., Epoetin alfa, Darbepoetin alfa) are FDA-approved drugs for the treatment of anemia resulting from chronic kidney disease or chemotherapy.

EPO signaling also drives activated platelet generation, expression of pro-thrombotic proteins, protection of non-hematopoietic cells against hypoxic stress, and nitric oxide production by the vascular epithelium (Lippi *et al.*, 2010; Sautina *et al.*, 2010; Lee *et al.*, 2020; Sergio and Rolando, 2022). To explain these diverse responses, we have proposed previously that EPO mediates the body's response to hemorrhage, simultaneously protecting tissues against reduced oxygen and promoting cessation of bleeding and the generation of new RBCs

38 (Burrill *et al.*, 2016; Lee *et al.*, 2021). The protection against stress is not limited to hypoxia; EPO
39 reduces cell death responses to a variety of stimuli. Due to its anti-apoptotic properties, there
40 has been interest in using EPO in disease states such as traumatic brain injury, myocardial
41 infarction, and neurodegenerative diseases such as ALS (Ghezzi and Brines, 2004; Grunfeld *et al.*,
42 2007; Gan *et al.*, 2012; Patel *et al.*, 2012; Hernández *et al.*, 2017; Robinson *et al.*, 2018). However,
43 the dose of EPO needed to activate protective signaling (~1-20 nM) is generally higher than the
44 dose necessary for its effects on erythroid and megakaryocytic cells (100-200 pM) (Anagnostou
45 *et al.*, 1990; Masuda *et al.*, 1993; Brines and Cerami, 2008). At these doses, the likelihood of off-
46 tissue EPO-R homodimer-driven effects, such as RBC and platelet generation, increases (Brines
47 and Cerami, 2008).

48 Tissue-protective signaling by EPO is thought to be mediated, at least in part, by a
49 heterodimer of EPO-R and CD131; however, the details of this signaling mode are unclear and
50 controversial (Brines *et al.*, 2004; Cheung Tung Shing *et al.*, 2018). CD131, the common beta
51 receptor (βc), is the beta subunit of the GM-CSF, IL-3, and IL-5 receptors and is crucial for the
52 differentiation of a diverse set of myeloid cell types (Scott and Begley, 1999). There is substantial
53 evidence that EPO-R and CD131 interact. Jubinsky *et al.* (Jubinsky *et al.*, 1997) first demonstrated
54 that CD131 functionally associates with EPO-R through co-immunoprecipitation experiments,
55 and Hanazono *et al.* (Hanazono *et al.*, 1995) observed phosphorylation of CD131 in response to
56 EPO. Moreover, Sautina *et al.* (Sautina *et al.*, 2010) found that co-immunoprecipitation of EPO-R
57 with anti-CD131 was enhanced by EPO. However, the structure of the full signaling complex and
58 how they interact is still unknown. Sautina *et al.* also found that VEGF receptor was co-
59 immunoprecipitated with EPO-R and anti-CD131 and may be part of the full complex (Sautina *et*
60 *al.*, 2010), and Cheung Tung Shing *et al.* (Cheung Tung Shing *et al.*, 2018) failed to find evidence
61 of an interaction between the extracellular domains of EPO-R and CD131 with and without EPO
62 using several biophysical binding assays (including surface plasmon resonance, microscale
63 thermophoresis and analytical size-exclusion chromatography). The findings of the
64 aforementioned studies are not necessarily in conflict with each other as an interaction could
65 still happen between the transmembrane segments of these receptors. This mechanism is
66 supported by work from He *et al.* that found that the extracellular domains of each receptor are

67 not required for downstream signaling through EPO-R/CD131 (He *et al.*, 2019). In sum, the
68 composition and structure of an EPO-R/CD131 complex and how these proteins interact to
69 induce downstream signaling is still controversial.

70 To selectively activate EPO-R/CD131 many groups have developed EPO derivatives that
71 putatively reduce or eliminate activation of homodimeric EPO-R, such as carbamylated EPO
72 (cEPO) (Leist *et al.*, 2004), EPO mutants with lower affinity for EPO-R (Leist *et al.*, 2004; Gan *et al.*,
73 2012; Lee *et al.*, 2021), smaller peptide derivatives of EPO (Brines *et al.*, 2008; Pankratova *et al.*,
74 2012; Ercan *et al.*, 2018; Cho *et al.*, 2022) or small EPO-mimetic peptides (Wrighton *et al.*, 1996;
75 He *et al.*, 2019). The most studied EPO alternative is carbamylated EPO, in which all amino
76 groups on the ten lysines have a carbamyl modification. cEPO has been proposed as a
77 neuroprotective therapeutic that does not produce red blood cells or platelets and is claimed to
78 signal only through EPO-R/CD131 and not through EPO-R homodimers (Leist *et al.*, 2004).
79 However, to the best of our knowledge, the quantitative effect of carbamylation on EPO's
80 binding to EPO receptor or CD131 has not been characterized (e.g., by surface plasmon
81 resonance), nor has its activity been rationalized in terms of solved structures of CD131 or EPO
82 and EPO-R.

83 Additionally, cEPO has the same plasma half-life as EPO itself – about eight hours
84 (Macdougall *et al.*, 1989). In the treatment of anemia, EPO can be used intermittently because
85 treatment produces a burst of erythroid progenitor activity that produces red blood cells lasting
86 100 days. However, neuroprotection by EPO signaling may require continuous exposure, which
87 may require genetically fusing a hormone to a module that extends half-life such as albumin or
88 the Fc region of an antibody. Rational design of such an engineered protein would require a
89 structural understanding of how EPO, EPO-R and CD131 interact. The focus of the present work
90 is to explore the structure of the EPO-R/CD131 signaling complex at a level sufficient to
91 construct engineerable fusion proteins that will activate EPO-R/CD131 selectively over EPO-
92 R/EPO-R.

93

94 **Results**

95 **Rational design of tandem scFv proteins for selective activation of EPO-R/CD131**

96 We aimed to develop selective agonists of EPO-R/CD131 that do not activate EPO-
97 R/EPO-R. Given the mechanisms of complex formation of the GM-CSF receptor (Carr *et al.*, 2001;
98 Hansen *et al.*, 2008; Caveney *et al.*, 2024) and EPO-R/EPO-R (Watowich *et al.*, 1994, 1999; Syed *et*
99 *al.*, 1998), we hypothesized that binding EPO-R and CD131 using a bispecific molecule would be
100 sufficient for pathway activation through induced proximity. To explore how binding flexibility
101 and orientation may affect receptor activation, we designed three fusion proteins with distinct
102 structural configurations. Each protein is bispecific and designed to bind both EPO-R and
103 CD131. We first generated a tandem scFv, whereby two scFvs are joined by a linker to generate
104 a single-chain bispecific binder. This protein (denoted as TscFv) consists of two previously
105 reported high-affinity scFvs (Borges *et al.*, 2008; Moraga *et al.*, 2015; Panousis *et al.*, 2016)
106 connected with a flexible glycine, serine, and glutamic acid linker (**Figure 1A**). We then fused
107 either the entire TscFv or the individual scFvs to the fragment crystallizable domain (Fc) of
108 mouse IgG2a (**Figure 1A**) since Fc fusion can improve the stability, manufacturability, and serum
109 half-life profiles of biologics. The first Fc fusion protein is a bispecific antibody with each scFv
110 fused to one half of Fc (denoted as BsAb), and the second Fc fusion consists of the entire TscFv
111 linked to one half of Fc (denoted as TscFv-Fc) (**Figure 1A**). To ensure both halves of the
112 bispecific Fc fusion proteins are present, we used a previously published heterodimeric Fc
113 variant that favors heterodimer formation through electrostatic steering (Wang *et al.*, 2019). This
114 improves the likelihood of retaining both halves of Fc after purification. The desired

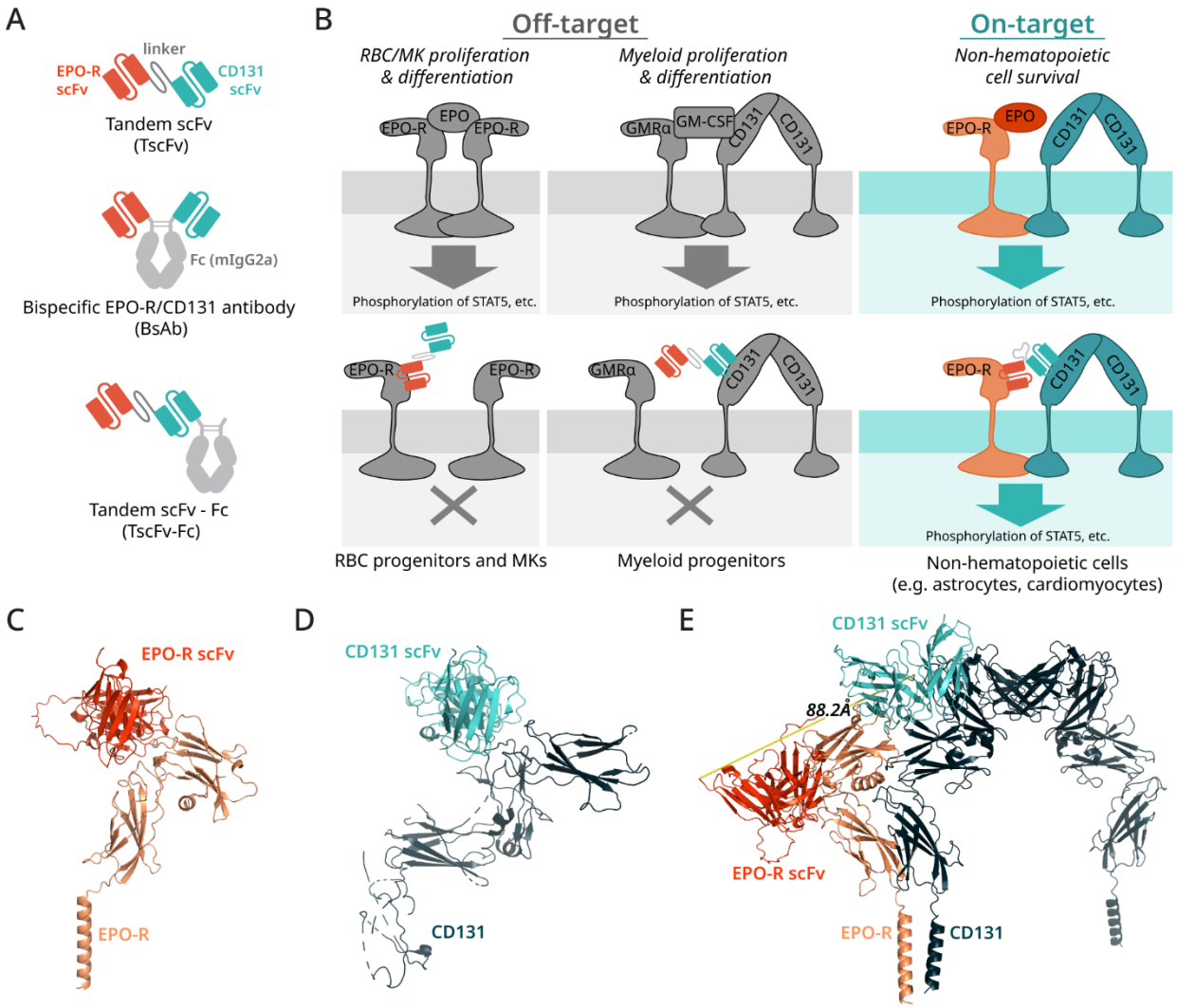

Figure 1. Design rationale for tandem scFvs that selectively bind EPO-R/CD131.

A. Schematic of the three bispecific fusion proteins explored in this work. Each consists of a previously published EPO-R binding scFv (Borges *et al.*, 2008; Moraga *et al.*, 2015) and a previously published CD131 binding scFv (Panousis *et al.*, 2016). The first protein (TscFv) is a tandem scFv whereby the EPO-R scFv and the CD131 scFv are joined by a long linker to make a single chain, bispecific binder. The other two proteins consist of the binding moieties fused to the fragment crystallizable (Fc) region of mouse IgG2a. Fusion to Fc is expected to enhance half-life due to an increase in size (and therefore a decrease in the rate of renal clearance) and FcRn-mediated recycling (Kontermann, 2011). One Fc fusion consists of the scFvs individually fused to the N terminus of Fc, forming a bispecific antibody (BsAb), and the other consists of the entire TscFv fused to one half of Fc (TscFv-Fc). **B.** Schematic of endogenous signaling through EPO-R and CD131 compared to the desired pathway activation by our fusion proteins. EPO naturally signals through either homodimeric EPO-R (which mediates RBC and platelet generation) or EPO-R/CD131. Our fusion proteins are designed to eliminate the activation of EPO-R homodimers to mimic EPO-induced activation of EPO-R/CD131 with enhanced selectivity. **C.** Solved structure (PDB 4y5y) of the EPO-R scFv bound to EPO-R (Moraga *et al.*, 2015) **D.**

Solved structure of the CD131 scFv (PDB 5dwu) bound to one monomer of CD131 (Panousis *et al.*, 2016)**. E.** Alphafold 3 (Abramson *et al.*, 2024) and PyMOL model of the potential structure of the tandem scFv in complex with EPO-R/CD131. We used Alphafold 3 to predict the interaction of each scFv with hEPO-R and $(CD131)_2$. Then we aligned both structures using the common structural elements (i.e., hEPO-R and $(CD131)_2$) using PyMOL. The resulting structure is one possible prediction of how EPO-R and CD131 may interact. In this model the C-terminus of the EPO-R scFv is 88 angstroms away from the N-terminus of the CD131 scFv. We used this model to design the linker to our tandem scFv, ensuring it could span that distance.

signaling of these three molecules is depicted in contrast to endogenous signaling of EPO in **Figure 1B**.

Since there is no structural information for a hypothetical EPO-R/CD131 complex, we used available structural data of the scFvs binding to their respective receptors (**Figure 1C, 1D**) and AlphaFold 3 (Abramson *et al.*, 2024) to model the potential interaction of EPO-R/CD131 and TscFv (**Figure 1E**). Specifically, we first generated one model of anti-EPO-R/EPO-R/$(CD131)_2$, and a separate model of anti-CD131/EPO-R/$(CD131)_2$ using AlphaFold. We included two copies of CD131 since it naturally forms a non-signaling dimer in which the two transmembrane segments are separated by 90-140 Å (Carr *et al.*, 2001). In the two predicted complexes, EPO-R and $(CD131)_2$ have a similar geometry as in these structures. We aligned the complexes using PyMol so that the EPO-R and $(CD131)_2$ molecules in each model were maximally aligned, and then we inferred the relationship of the anti-EPO-R and anti-CD131 scFvs as a hypothetical geometry to be tested. Using this structure, we measured an approximate distance the scFvs could be in the fully formed complex, which informed our linker design. In this model, the C terminus of the EPO-R scFv is positioned 88.2 Å from the N terminus of the CD131 scFv (**Figure 1E**). Assuming an average amino acid contour length of 4 Å, (Ainavarapu *et al.*, 2006) this distance could be covered by a ≥22 amino acid (aa) linker. Therefore, our first TscFv design connects the EPO-R and CD131 scFvs with a 23 aa linker consisting of glycine, serine and glutamic acid to allow unimpeded long-range movement of each scFv and to increase overall solubility. The spacing of the scFvs in BsAb also should be sufficient to allow simultaneous binding since the distance between the Fabs of wildtype mouse IgG2a, is 117 ± 37 Å (Sosnick *et al.*, 1992).

158 The proposed model has features that are consistent with past observations about a
159 putative EPO-R/CD131 interaction. In the structural model, EPO-R associates with CD131 along a
160 face away from the EPO binding site, such that if EPO were bound to EPO-R in this complex, EPO
161 would not contact CD131. Such an interaction might nonetheless be promoted by EPO if we
162 envision that unliganded EPO-R exists primarily in a self-inhibited dimeric state implied by the
163 crystal structure (Livnah *et al.*, 1999) in equilibrium with an unliganded monomer. In the
164 unliganded dimer, EPO-R interacts with itself by the same surface that binds to EPO, and the
165 geometry of this interaction would force the EPO-R dimer to lie flat against the cell membrane.
166 Additionally, EPO would bind to the unliganded monomer and prevent re-formation of the
167 inactive dimer so the EPO/EPO-R complex could then interact with CD131. This model would
168 explain how high concentrations of EPO variants with a mutation in the "weak face" surface that
169 interacts with the second EPO-R could still signal through EPO-R and CD131. We explore this
170 model further in the Supporting Information (**Figure S1, S2**). Concurrently, we also generated
171 models using AlphaFold 3 for interacting extracellular domains of EPO-R and CD131, with and
172 without EPO or the TscFv (**Figure S3**). These models all showed EPO-R in proximity to the most
173 membrane-proximal domain of CD131, but differed in specific contacts. This suggests that the
174 extracellular domains of EPO-R and CD131 might interact weakly or not at all, and that their
175 interaction may require contacts between the transmembrane and/or intracellular domains.

176 We first assessed whether fusion of the scFvs to each other or to Fc would hinder their
177 binding. We expressed and purified each protein and verified the presence of heterodimers in
178 the case of the Fc fusions (**Figure S4E and S4F**). Then, we determined whether the constructs
179 bind EPO-R and CD131 by elisa. TscFv bound both receptors with similar EC_{50}s (**Figure 2A, 2B**),
180 demonstrating that TscFv folds properly and the tandem scFv format is flexible enough to allow
181 proper receptor binding.

182 In contrast, both Fc fusion constructs (BsAb and TscFv-Fc) had at least an order of
183 magnitude lower apparent binding affinity for either receptor when compared to TscFv.

184

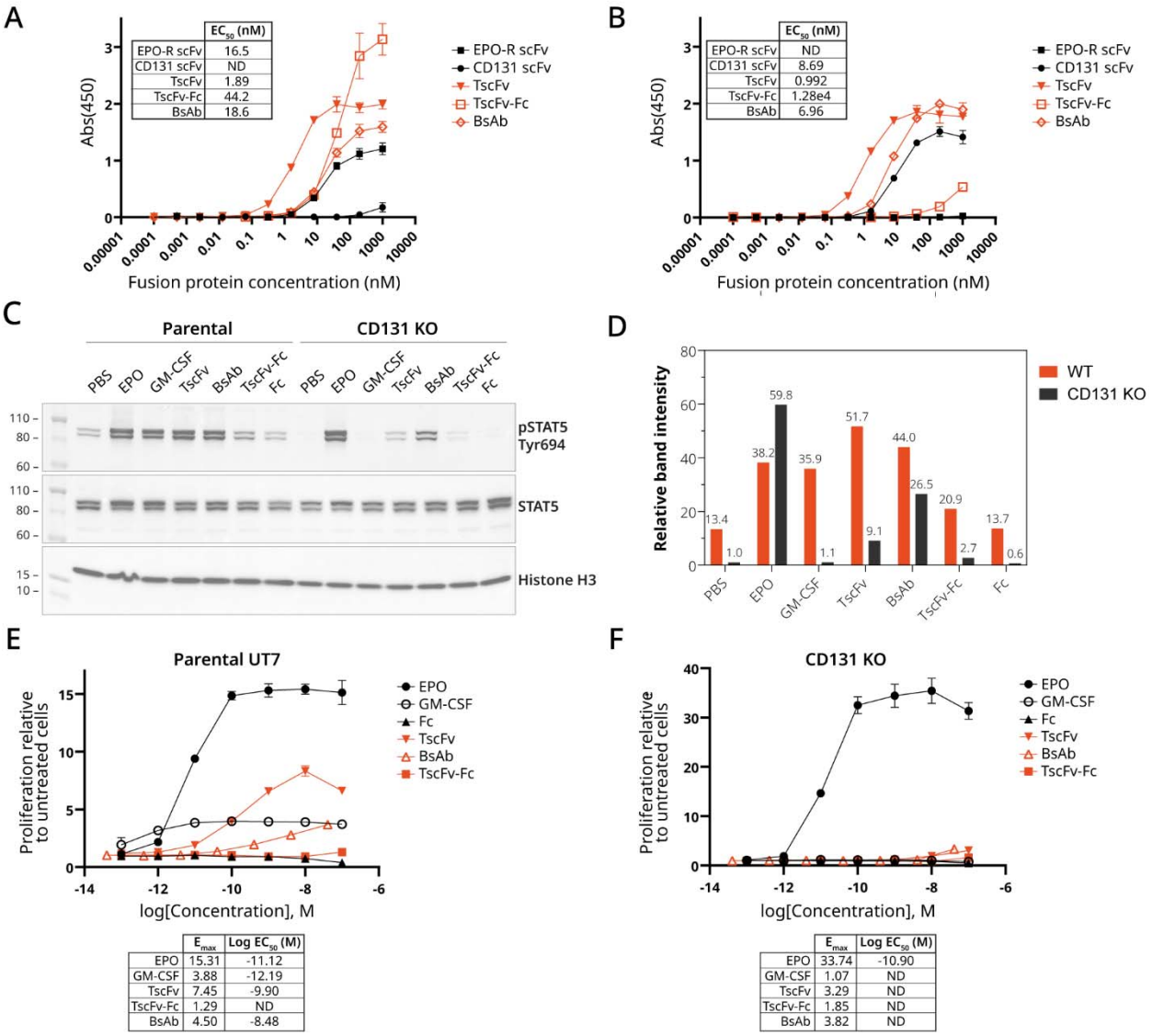

	EC_{50} (nM)
EPO-R scFv	16.5
CD131 scFv	ND
TscFv	1.89
TscFv-Fc	44.2
BsAb	18.6

	EC_{50} (nM)
EPO-R scFv	ND
CD131 scFv	8.69
TscFv	0.992
TscFv-Fc	1.28e4
BsAb	6.96

	E_{max}	Log EC_{50} (M)
EPO	15.31	-11.12
GM-CSF	3.88	-12.19
TscFv	7.45	-9.90
TscFv-Fc	1.29	ND
BsAb	4.50	-8.48

	E_{max}	Log EC_{50} (M)
EPO	33.74	-10.90
GM-CSF	1.07	ND
TscFv	3.29	ND
TscFv-Fc	1.85	ND
BsAb	3.82	ND

Figure 2. Tandem scFv and BsAb bind EPO-R and CD131 and activate downstream CD131-dependent STAT5 phosphorylation and proliferation in UT-7-ES1. A-B. Elisa of each of the bispecific proteins binding to EPO-R or CD131. Recombinant **A.** EPO-R or **B.** CD131 were used to coat elisa plates and relative binding of each protein to both receptors was determined. Elisa data are reported as mean A_{450} ± SD of three replicates. EC_{50} values were calculated using GraphPad Prism. **C.** All fusion proteins activated the phosphorylation of STAT5 at Tyr694. UT-7 EPO S1 (UT-7-ES1) is a cell line that is dependent on signaling through EPO-R/EPO-R, EPO-R/CD131, or GMCSFRα/CD131 to survive. Parental UT-7-ES1 or a UT-7-ES1 clonal CD131 KO line were FBS starved overnight, treated with 100 nM proteins for 15 min, and lysed in the presence of protease and phosphatase inhibitors. Proteins were run by SDS-PAGE and visualized by western blot with the designated antibodies. **D.** Quantification of the density of sample bands in **C** relative to PBS treated sample from the CD131 KO line. **E.** TscFv and BsAb support growth of parental UT-7-ES1. UT-7-ES1 were cytokine starved overnight, treated with the designated proteins and viability was measured 72 hrs

197 later. **F.** TscFv and BsAb do not support growth of UT-7-ES1 with CD131 KO. A clonal CD131 KO UT-7-ES1 line was
198 cytokine starved overnight, treated with the designated proteins and viability was measured 72 hrs later. Proliferation
199 data are reported as proliferation relative to untreated cells and are represented by mean luminescence ± SD of three
200 replicates. EC_{50} values were calculated using GraphPad Prism.

201

202 TscFv-Fc and BsAb exhibited similar binding to EPO-R (**Figure 2A**), with EC_{50}s of 44.2 nM and
203 18.6 nM respectively. However, TscFv-Fc has severely impaired binding (12,800 nM) to CD131
204 compared to the other proteins (**Figure 2B**), suggesting steric hindrance from the Fc or the lack
205 of flexibility of that scFv due to its fusion to the C terminus to Fc. The diminished binding of the
206 BsAb and TscFv-Fc molecules is explained further in **Supplementary Figure 5**. Overall, TscFv
207 and BsAb are expressed and purified to titers of 5-10 mg/L and bind both EPO-R and CD131 as
208 expected.

209

210 **EPO-R/CD131 tandem scFv and BsAb induce CD131-dependent STAT5 signaling and**
211 **proliferation in UT-7-ES1 cells**

212 To determine if our proteins could activate EPO-R signaling, we first assessed their ability
213 to support the growth of an EPO-responsive cell line, UT-7 EPO S1 (herein referred to as UT-7-
214 ES1). UT-7-ES1 (Shimomura *et al.*, 1992; Komatsu *et al.*, 1993) expresses both EPO-R and CD131
215 and is dependent on either EPO or GM-CSF for growth. Consequently, signaling from EPO-
216 R/EPO-R, EPO-R/CD131, or GM-CSFRα/CD131 could be sufficient to support proliferation of
217 these cells. Western blotting to detect phosphorylated STAT5 (Tyr694) revealed faint bands at
218 the correct molecular weight for STAT5A and STAT5B in the unstimulated cell line, indicating
219 some level of basal STAT5 activation in UT-7-ES1.

220 As expected, the natural cytokines that support cell proliferation, EPO or GM-CSF,
221 induced approximately 3-fold higher STAT5 phosphorylation than both negative controls (PBS
222 and Fc) (**Figure 2C, 2D**). Both TscFv and BsAb also activated STAT5 phosphorylation, inducing 3
223 to 4-fold higher phosphorylation of STAT5 when compared to the PBS or Fc treated samples
224 respectively (**Figure 2C, 2D**). TscFv-Fc elicited less STAT5 phosphorylation than TscFv and BsAb

225 (**Figure 2C, 2D**), possibly due to its impaired CD131 binding at this concentration compared to
226 TscFv and BsAb (**Figure 2B**). In sum, EPO, GM-CSF, TscFv, and BsAb all induced STAT5
227 phosphorylation in the parental UT-7-ES1 cell line.

228 Since STAT5 phosphorylation can be activated through either EPO-R/EPO-R or EPO-
229 R/CD131, we assessed whether CD131 expression was required. We used standard CRISPR-Cas9
230 gene-editing to generate a clonal UT-7-ES1 CD131 knockout (Clone C; **Figure S6**). This knockout
231 line has a 25-bp deletion in exon 4 (**Figure S6D**) which is in the first domain of CD131, the main
232 extracellular domain that interacts with GM-CSF. A western blot using an anti-CD131 antibody
233 against parental UT-7-ES1 revealed three bands (**Figure S6A**), and the two high-molecular
234 weight bands are knocked out in the UT-7-ES1 Clone C cell line (**Figure S6B**). In this knockout
235 line, CD131 KO eliminated the basal STAT5 phosphorylation of untreated samples that we
236 observed in parental UT-7-ES1 (**Figure 2C, 2D**).

237 As expected, treatment with GM-CSF no longer induced STAT5 phosphorylation in UT-7-
238 ES1 clone C (**Figure 2C, 2D**), verifying functional knockout of CD131 in this cell line. Also as
239 expected, STAT5 phosphorylation induced by EPO is not reduced in the CD131 KO cell line since
240 signaling can still occur through homodimeric EPO-R (**Figure 2C, 2D**). Each engineered
241 bispecific construct induced some level of STAT5 phosphorylation in this line despite the lack of
242 functional CD131. However, STAT5 phosphorylation was markedly reduced, and all three
243 bispecific constructs induced less STAT5 phosphorylation than EPO (**Figure 2C, 2D**). The weak
244 remaining induction of STAT5 phosphorylation by our proteins could be due to binding of the
245 anti-CD131 scFv element to a fragment of CD131 in the clone C cell line (**Figure S6B, S6D**).

246 Next, we determined whether the stimulation provided by our fusion proteins was able
247 to support proliferation of UT-7-ES1. As expected, cytokine-starved parental UT-7-ES1 cells
248 showed dose-dependent survival after treatment with EPO or GM-CSF (**Figure 2E**). TscFv
249 induced strong dose-dependent survival of UT-7-ES1, although the potency and efficacy was
250 less than EPO (**Figure 2E**). This could be because EPO can induce signaling through both EPO-R
251 homodimers and EPO-R/CD131, while TscFv should only be able to signal through EPO-
252 R/CD131. BsAb also supported dose-dependent survival of UT-7-ES1. However, BsAb is less

253 potent than TscFv and only supports modest growth at the three highest concentrations tested.
254 Finally, consistent with the binding and signaling data, TscFv-Fc does not support proliferation
255 of UT-7-ES1. These data demonstrate that the natural ligands, EPO and GM-CSF, and our
256 proteins, TscFv and BsAb, are able to support dose-dependent proliferation of UT-7-ES1.

257 In the UT-7-ES1 CD131 KO line, EPO, but not GM-CSF, supported proliferation (**Figures**
258 **2F, S6C**), further verifying the functional knockout of CD131. However, in contrast to the
259 parental UT-7-ES1 cell line, CD131 KO cells treated with TscFv and BsAb did not proliferate at
260 any dose tested (**Figure 2F**). TscFv-Fc, did not support proliferation of either Parental or CD131
261 KO UT-7-ES1 (**Figure 2E, 2F**) which is consistent with the STAT5 phosphorylation (**Figure 2C,**
262 **2D**) and CD131 binding (**Figure 2B**) data. In sum, TscFV and BsAb induce CD131-dependent
263 STAT5 phosphorylation and proliferation in UT-7-ES1.

264

265 **EPO-R/CD131 tandem scFv and BsAb selectively activate EPO-R/CD131 but not EPO-**
266 **R/EPO-R**

267 To further investigate the pathway selectivity of the tandem scFv proteins, we next
268 compared treatment responses in engineered human embryonic kidney (HEK293T) cell lines
269 overexpressing EPO-R, CD131 or both EPO-R and CD131 (**Figures 3A, S7**). Parental HEK293T do
270 not express either EPO-R or CD131. We transduced HEK293T cells with lentiviral expression
271 constructs encoding EPO-R, CD131 or both receptors to yield pooled cell lines with stable
272 receptor expression. Each cell line was transduced independently, and they are not lineally
273 related (i.e., the cell line expressing both EPO-R and CD131 is not a derivative of either the EPO-
274 R or CD131 only line). Both receptors were FLAG-tagged to verify expression of each receptor
275 (**Figures 3B, 3C, S7**). The cell line expressing EPO-R can only signal through homodimeric EPO-
276 R, while the line that expresses both EPO-R and CD131 can signal through both homodimeric
277 EPO-R and EPO-R/CD131 signaling. Comparing the treatment responses of these two cell lines
278 enables the determination of selectivity by showing whether CD131 is required for activation
279 (**Figure 3A**).

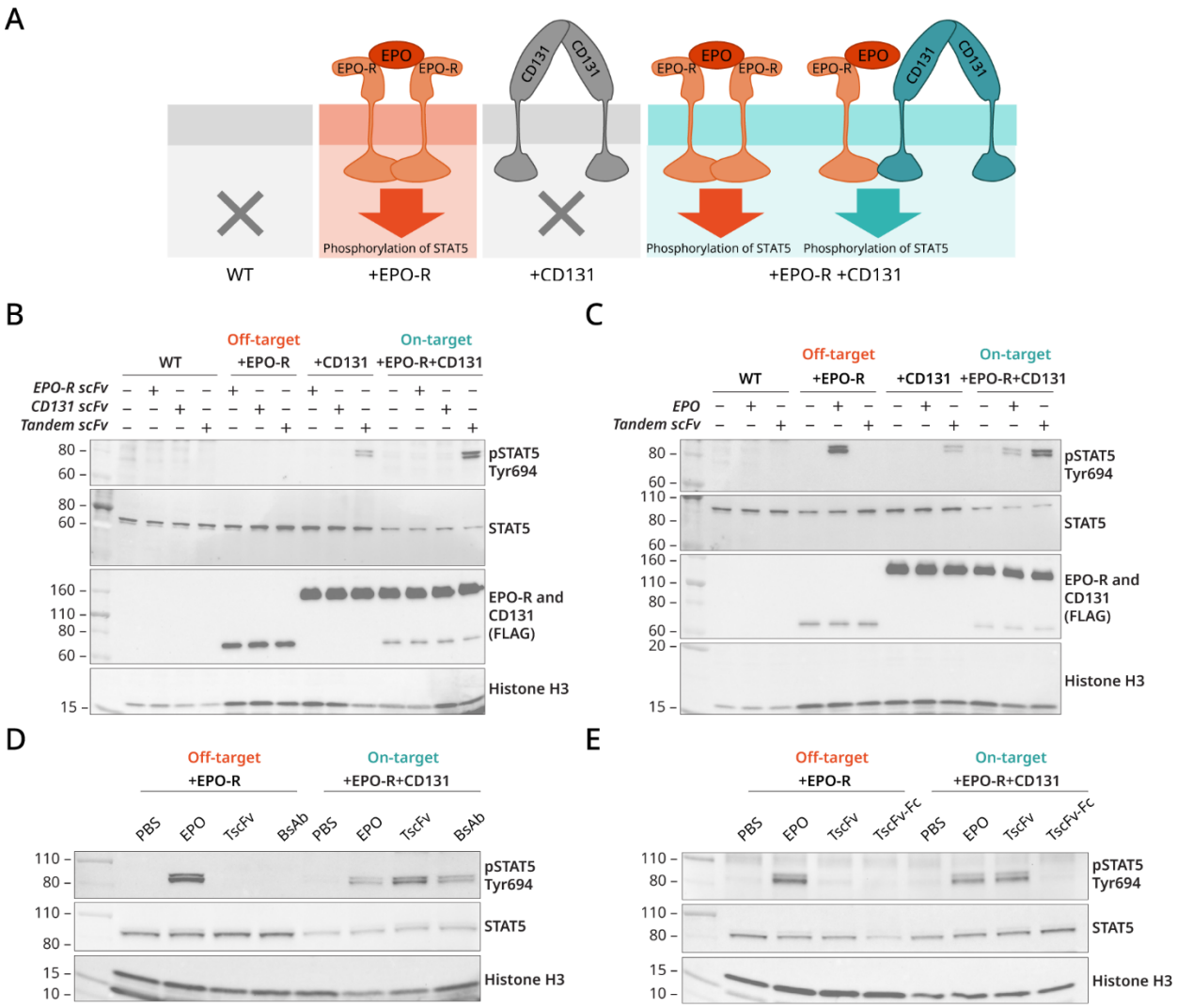

Figure 3. Tandem scFv and BsAb selectively activate STAT5 phosphorylation downstream of EPO-R/CD131 but not homodimeric EPO-R. A. Schematic of signaling in each overexpression line. HEK293T cells were stably transduced with FLAG-tagged expression constructs of either hEPO-R, hCD131, or both. Comparing the response between cells with both EPO-R and CD131 (which will have EPO-R/EPO-R and EPO-R/CD131 signaling) to cells with only EPO-R (which only can signal through EPO-R/EPO-R) can illuminate EPO-R/CD131-specific signaling. **B-E.** Cells were FBS starved overnight, treated with the designated proteins at 100 nM for 15 min, and lysed in the presence of protease and phosphatase inhibitors. Proteins were run by SDS-PAGE and visualized by western blot with the designated antibodies. **B.** TscFv, but not the individual scFvs, triggers CD131-dependent STAT5 phosphorylation. **C.** TscFv has a different signaling profile than EPO and does not activate EPO-R/EPO-R. **D.** BsAb is also only able to induce STAT5 phosphorylation in cells that express CD131. **E.** TscFv-Fc does not activate STAT5 phosphorylation downstream of EPO-R/EPO-R nor EPO-R/CD131.

293 Additionally, unlike UT-7-ES1, HEK293T do not express the alpha subunit of any CD131 receptor,
294 so treatment response in these lines cannot be complicated by activation of related CD131-
295 containing receptors.

296 As expected, the unfused anti-EPO-R and anti-CD131 scFvs did not induce STAT5
297 phosphorylation in any cell line (**Figure 3B**), most likely due to the inability of a monomeric scFv
298 to induce receptor dimerization. Also as expected, EPO induced STAT5 phosphorylation in both
299 EPO-R and EPO-R/CD131 expressing cell lines (**Figure 3C**), confirming functional EPO-R
300 signaling in these lines. However, in contrast, TscFv induced strong STAT5 phosphorylation only
301 in cells that express both EPO-R and CD131, but not the EPO-R-only cell line (**Figure 3B**),
302 demonstrating specificity to heterodimeric EPO-R signaling. TscFv also induced weak STAT5
303 phosphorylation in the CD131-only overexpression line (**Figure 3B**), which remains unexplained,
304 but we believe it is a cell-line specific effect. To determine if this effect was cell-line dependent,
305 we separately constructed a HEK293T cell line expressing a V5-tagged CD131 that expresses less
306 CD131 (**Figure S7**). In this line which only expresses CD131, TscFv did not induce detectable
307 STAT5 phosphorylation (**Figure S8**). Finally, BsAb also demonstrated specificity as treatment
308 only induced STAT5 phosphorylation in the cell line expressing EPO-R and CD131 (**Figure 3D**).

309 To determine if simply the presence of both scFvs was sufficient for signaling, we treated
310 cells with an equimolar mix of the EPO-R and CD131 scFvs. An equimolar mix of the scFvs did
311 not induce STAT5 signaling in either the EPO-R only or EPO-R and CD131 overexpression cell
312 lines (**Figure S9**), suggesting simultaneous binding and linking of both receptors is necessary.
313 Finally, consistent with the signaling and binding data, TscFv-Fc was unable to activate STAT5
314 phosphorylation in either line at the same dose (**Figure 3E**). In conclusion, TscFv and BsAb are
315 most active in the EPO-R/CD131 cell line and not active in cells expressing only EPO-R, and the
316 bispecific nature of TscFv and BsAb is necessary for activity. Therefore, induced proximity of
317 EPO-R and CD131 by a single bispecific molecule appears to be sufficient for EPO-R/CD131
318 activation.

319

320 **Decreasing linker length between anti-EPO-R and anti-CD131 scFvs in TscFv modifies**
321 **signaling**

322 Based on the EPO-R/CD131/tandem scFv structural model (**Figure 1E**), we hypothesized
323 that shortening the inter-scFv linker would reduce or eliminate downstream signaling.
324 Specifically, in our model, the C-terminus of the anti-EPO-R scFv and the N-terminus of the anti-
325 CD131 scFv are separated by 88 Å. The 23 aa linker in TscFv (denoted GS-L, **Figure 4**) can cover
326 this distance when fully extended. If this model is correct, shortening the linker would likely
327 reduce or eliminate signaling because the proper geometry of EPO-R and CD131 would be
328 entropically unfavored or sterically infeasible.

329 We designed several new TscFv variants with linkers of differing length and rigidity (Chen
330 *et al.*, 2013). Specifically, a tandem scFv with a 7-amino acid linker between the anti-EPO-R scFv
331 and the anti-CD131 scFv (SF for short, flexible); a tandem scFv with a 23-amino acid rigid linker
332 between the scFvs (LR for long, rigid); a tandem scFv with a 7-amino acid rigid linker between
333 scFvs (SR for short, rigid); and a tandem scFv with no linker (NL) (**Figure 4**). We also rearranged
334 the variable domains of the anti-EPO-R scFv in one variant so that its linker attachment point is
335 further away from the anti-CD131 scFv ("Swap") (**Figure 4**).

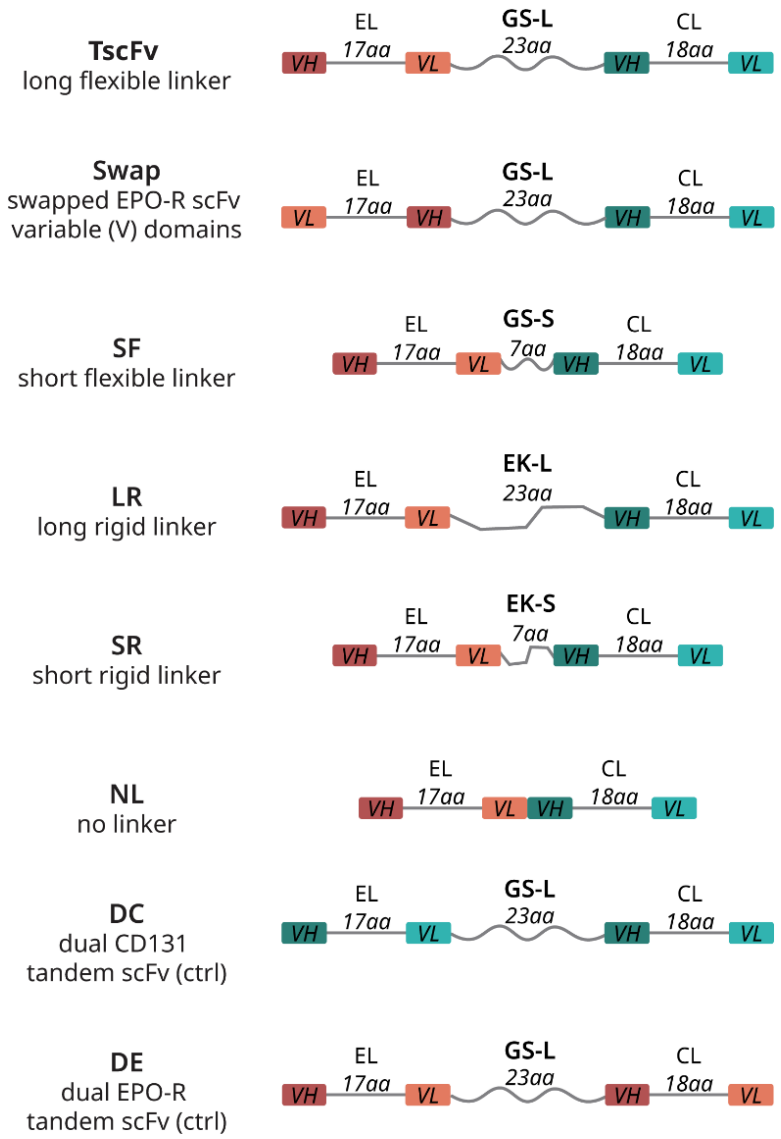

Linker	Sequence
EL	GGGGSGGGGSSGGGGSS
GS-L	GSGEGGSESSGEGSGESSGEGSG
CL	GSGGGSSSGGSGSSGGSG
GS-S	ESSGEGS
EK-L	EAAAKEAAAKEAAAKEAAAKEAA
EK-S	EAAAKEA

Figure 4. Design of tandem scFv linker and domain variants. A. Variants were made of TscFv with changes to the linker connecting the two scFvs or the variable (V) domain order of the EPO-R scFv. Two control tandem scFvs (TscFv-DE and TscFv-DC) were also constructed to test whether signaling was due to the bispecific binding of TscFv, not just the presence of two scFvs. The linkers connecting the variable domains of each scFv (EL and CL) were kept the same in all constructs. The sequence of each linker is listed. Abbreviations: VH=heavy chain, VL=light chain, GS=Glycine and serine linker, EK=Glutamic acid and lysine linker, L=long, S=short.

343 The linker variants with no linker, shorter linkers, or more rigid linkers (NL, SF, SR, LR)
344 induced two to four-fold less STAT5 phosphorylation in parental UT-7-ES1 compared to the
345 original TscFv (which has a long, flexible linker) (**Figure 5A, 5B**). STAT5 phosphorylation in the
346 UT-7-ES1 CD131 KO cell line was greatly reduced or completely eliminated for all of the linker
347 variants (except "Swap"), suggesting CD131 dependent signaling (**Figure 5C, 5D**). Residual
348 activity of these constructs could be explained according to the model depicted in
349 **Supplementary Figure 10**. Unexpectedly, the "Swap" tandem scFv induced more STAT5
350 phosphorylation in comparison to TscFv in the UT-7-ES1 CD131 KO line (**Figure 5C, 5D**). We
351 believe this is due to the linker length between the two scFvs, which may force dimerization of
352 the anti-EPO-R scFv and enable some level of homodimeric EPO-R signaling (diagrammed in
353 **Supplementary Figure 11**).

354 All linker variants also induced STAT5 phosphorylation in the HEK293T line that expresses
355 EPO-R and CD131 (**Figure 5E, 5F**). TscFv variants with longer linkers (TscFv, LR) were more
356 efficacious than those with shorter linkers, consistent with the UT-7-ES1 results. We also
357 designed two tandem scFv controls, DC (dual anti-CD131 scFv) and DE (dual anti-EPO-R scFv)),
358 which each consist of two of the same scFv connected by a long, flexible linker (**Figure 4**). Since
359 it has two EPO-R binding moieties, DE should signal through EPO-R/EPO-R, while the dual anti-
360 CD131 scFv (DC) should not. As expected, DE induced a level of STAT5 phosphorylation that is
361 similar to EPO, and DC did not induce strong STAT5 phosphorylation (**Figure 5E, 5F**).
362 Comparison of the response induced by TscFv, DE, and DC further suggests that the induced
363 STAT5 phosphorylation is not due to the presence of two linked scFvs but is specific to the
364 presence of both EPO-R and CD131 binding moieties in the same molecule (**Figures 5E, 5F,**
365 **S12**).

366 Finally, we tested the ability of the TscFv linker variants to support proliferation of UT-7-
367 ES1. The maximum response (E_{max}) of the variants varies markedly (**Figure 5G**). TscFv variants
368 with shorter linkers induced less proliferation compared to the original (**Figure 5G**). As expected,
369 DE supported cell proliferation since it can signal through homodimeric EPO-R in the UT-7-ES1
370 CD131 KO cell line (**Figure S12**). However, all of the linker variants induced little or no
371 proliferation in the UT-7-ES1 CD131 KO cell line (**Figure 5H**), further demonstrating their

372 specificity. Altogether, these data indicate that TscFv and its variants require CD131 to support
373 UT-7-ES1 proliferation, suggesting they are more selective for EPO-R/CD131 than natural EPO.

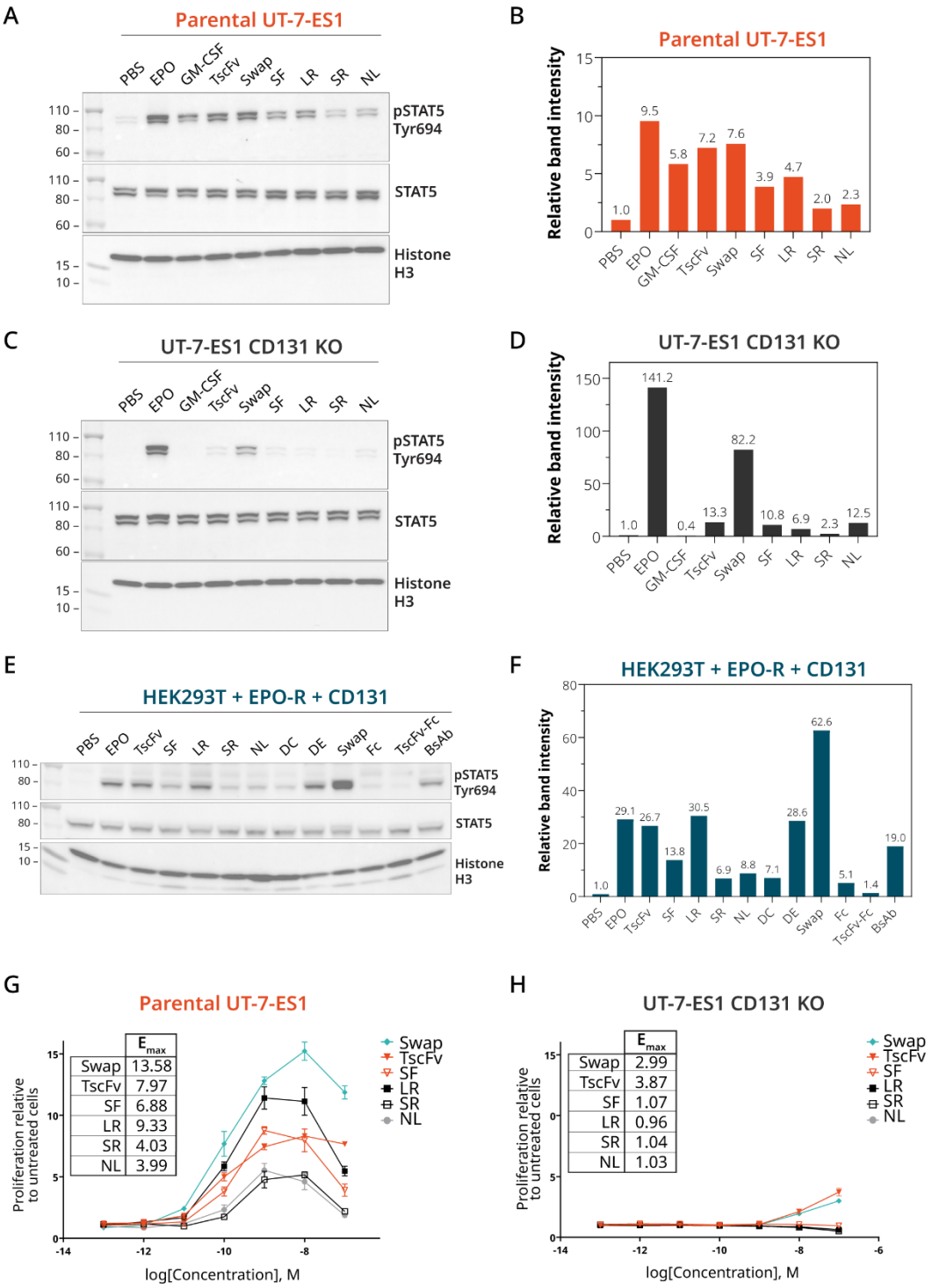

Figure 5. Decreased linker length between EPO-R and CD131 scFvs decreases signaling of tandem scFv variants. A, C. UT-7-ES1 or UT-7-ES1 CD131 KO cells were FBS starved overnight, treated with the designated proteins at 100 nM for 15 min, and lysed in the presence of protease and phosphatase inhibitors. Proteins were run by SDS-PAGE and visualized by western blot with the designated antibodies. **B, D.** Band densities of STAT5 phosphorylated at Tyr694 in **A** and **C** were quantified and plotted relative to the density of the PBS-treated control

380 bands. **E.** HEK293T overexpressing EPO-R and CD131 were FBS starved overnight, treated with the designated
381 proteins at 100 nM for 15 min, and lysed in the presence of protease and phosphatase inhibitors. Proteins were run by
382 SDS-PAGE and visualized by western blot with the designated antibodies. **F.** Band densities of **E** relative to the PBS-
383 treated control sample. **G.** Parental UT-7-ES1 lines were cytokine starved overnight, treated with the designated
384 proteins at 100 nM and viability was measured 72 hrs later. TscFv and its variants are able to support UT-7-ES1
385 proliferation, but variants with decreased linker length induce less proliferation. **H.** UT-7-ES1 CD131 KO cells were
386 treated as in **G** and viability was measured 72 hrs later. TscFv and linker variants are unable to support proliferation of
387 UT-7-ES1 when CD131 is knocked out. Proliferation data are reported as proliferation relative to untreated cells and
388 are represented by mean luminescence ± SD of three replicates. E_{max} values were calculated using GraphPad Prism.

389

390 ## Discussion

391 Signaling through a combination of EPO-R and CD131 is thought to promote resistance
392 to cell stress, such as neurons exposed to hypoxia or traumatic brain injury. In this study, we
393 developed the first selective EPO-R/CD131 agonists. Previous work identified antibodies that
394 bind to EPO-R (Lim *et al.*, 2010; Moraga *et al.*, 2015) or CD131 (Panousis *et al.*, 2016) and solved
395 the structure of these scFvs in complex with their target antigen. We used AlphaFold 3
396 (Abramson *et al.*, 2024) to construct a model of an EPO-R/CD131 signaling complex, determined
397 where the V regions from the anti-EPO-R and anti-CD131 antibodies would bind, and then
398 designed and expressed a tandem scFv (TscFv) consisting of an anti-EPO-R scFv, an anti-CD131
399 scFv, and a linker long enough to connect them. Additionally, we constructed a bispecific
400 antibody (BsAb) by fusing the scFvs to a heterodimeric Fc. TscFv and BsAb induced STAT5
401 phosphorylation through activation of EPO-R/CD131, without engaging EPO-R/EPO-R (**Figure 2,**
402 **Figure 3**) and also induced cell proliferation of UT-7-ES1 in a CD131-dependent manner (**Figure**
403 **2, Figure 4)**. Finally, we demonstrate that shortening the linker between the scFvs reduced
404 signaling in a manner consistent with the predicted structural model of EPO-R/CD131. These
405 proteins provide proof of concept for design of selective EPO-R/CD131 agonists and lay a
406 foundation for the development of a clinical-grade EPO-R/CD131 biologic drug.

407 EPO and EPO variants can prevent cell death of non-hematopoietic cells in the face of
408 cytotoxic agents or hypoxia in *in vitro* and *in vivo* models of neurodegeneration and trauma

409 (Ghezzi and Brines, 2004; Grunfeld *et al.*, 2007; Patel *et al.*, 2012; Ponce *et al.*, 2013; Noh *et al.*,
410 2014; Robinson *et al.*, 2018; Hemani *et al.*, 2021). However, the concentration needed to
411 generate this cell protective signaling (1-20 nM vs.100-200 pM for hematopoietic effects) would
412 lead to undesired effects, such as RBC and prothrombotic platelet generation, due to activation
413 of homodimeric EPO-R (Brines and Cerami, 2012). Previous efforts to make specifically tissue-
414 protective EPOs have centered around mutated or modified EPO, such as carbamylated EPO or
415 proteins with mutations in the face of EPO that mediates the weak interaction with EPO-R (Leist
416 *et al.*, 2004; Brines *et al.*, 2008; Gan *et al.*, 2012; Pankratova *et al.*, 2012; Cho *et al.*, 2022). These
417 molecules fortuitously happened to have desirable properties, without a clear mechanism by
418 which the EPO-R/CD131 signaling properties derive from the structure.

419 In this work, our strategy has been to construct molecules that bring EPO-R and CD131
420 together via scFvs that bind to each receptor. The best selective EPO-R/CD131 activator is a
421 single polypeptide chain tandem scFv consisting of an N-terminal scFv that binds to EPO-R
422 (Moraga *et al.*, 2015), a central 23-amino acid linker, and a C-terminal scFv that binds to CD131
423 (Panousis *et al.*, 2016), denoted TscFv. The design of this molecule was driven by a structurally
424 plausible AlphaFold 3 model of interacting EPO-R and CD131. However, the 23-amino acid linker
425 has a maximum extended length of about 100 Angstroms, so the molecule could accommodate
426 many possible configurations of EPO-R and CD131.

427 TscFv stimulated the growth of UT-7-ES1 in a CD131-dependent manner and was not
428 active in cells that only express EPO-R (**Figures 2E, 2F, 5G, 5H**). This is in contrast to a tandem
429 scFv consisting of two anti-EPO-R scFvs (denoted DE; **Figure 4, S12 ("DE")**), which can still
430 stimulate the growth of cells without CD131. These observations also suggest that TscFv
431 assembles as diagrammed, and does not form dimers in which two anti-EPO-R scFvs form a
432 diabody that could link two EPO-Rs. Specific signaling through EPO-R/CD131 was observed in
433 two paired cell lines: UT-7-ES1 parental cells compared to UT-7-ES1 CD131-knockout cells
434 (**Figures 2, 5**), and HEK293T cells engineered to express EPO-R only or both EPO-R and CD131
435 (**Figures 3, 5**). When parental UT-7-ES1 cells were treated with TscFv, the level of STAT5
436 phosphorylation was comparable to that induced by EPO, while in the UT-7-ES1 CD131

437 knockout cells, only a trace of STAT5 phosphorylation was observed. The UT-7-ES1 parental cells
438 proliferated in response to TscFv and its variants (**Figures 4, 5G, 5H**), while the UT-7-ES1 CD131
439 knockout cells did not proliferate at all in response to any of these proteins (**Figures 2E, 2F, 5G,**
440 **5H**). Similarly, TscFv stimulated STAT5 phosphorylation in HEK293T cells expressing both EPO-R
441 and CD131, but not cells expressing only EPO-R (**Figure 3**).

442 Based on our results, we envision that a practical therapeutic protein that specifically
443 activates EPO-R/CD131 complexes could be constructed. Such proteins could be used to treat
444 neurological disorders, such as traumatic brain injury (Robinson *et al.*, 2018), ALS (Noh *et al.*,
445 2014; Lauria *et al.*, 2015), and possibly also Alzheimer's disease (Kalluru *et al.*, 2024). To be useful
446 in these chronic conditions, such a molecule should not induce autoantibodies to endogenous
447 EPO and should have a long plasma half-life. Repeated administration of EPO-based scaffolds
448 introduces the risk of triggering an autoimmune response to endogenous EPO (Casadevall *et al.*,
449 2005; Tamilvanan *et al.*, 2010). In contrast, our constructs will not induce autoantibody
450 production to EPO as they differ significantly in structure.

451 Pharmacokinetics represents a further challenge. Human EPO has a plasma half-live of
452 only a few hours, but nonetheless has been a successful drug since the major use of EPO is to
453 treat kidney failure patients who are on dialysis (Kalantar-Zadeh, 2017). Typically, such patients
454 undergo dialysis three times per week, and IV administration of EPO through the line already set
455 up for the dialysis is practical in this context. Moreover, in treating anemia it is not essential to
456 have continuous exposure to EPO, as long as there is production of red blood cells, which have a
457 lifetime of about 100 days. However, in treating a neurodegenerative disorder, continuous EPO
458 signaling may be necessary. Boesch *et al.* (Boesch *et al.*, 2007, 2008) performed a pilot clinical
459 trial on 12 patients with Friedreich's ataxia and saw a favorable effect on biomarkers; the
460 patients received EPO three times per week, the same dose that a dialysis patient would receive,
461 but a dose that likely enhances thrombotic events due to induction of EPO-R/EPO-R signaling.
462 In subsequent trials of EPO and carbamylated EPO for Friedreich's ataxia, patients were dosed
463 once every two to three weeks (Mariotti *et al.*, 2012; Boesch *et al.*, 2014). Additionally, Lauria *et*
464 *al.* (Lauria *et al.*, 2015) clinically tested EPO as a treatment for ALS, also dosing once per two

465 weeks. Given EPO's plasma half-life in humans of about 8 hrs, the patients' nervous systems
466 would be unprotected for most of each dosing period. Our anti-EPO-R/anti-CD131 tandem scFv
467 has a much larger Stoke's radius than EPO and carbamylated EPO, which should lead to a
468 superior plasma half-life. Moreover, current fusion protein technologies allow for profound
469 extension of plasma half-life, such that high levels of a protein drug can be maintained for
470 several weeks. With this in mind, we designed BsAb, which consists of the EPO-R and CD131
471 scFvs fused to Fc. BsAb is also selective for EPO-R/CD131 and will likely have a superior plasma
472 half-life due to its size and Fc receptor (FcRn)-mediated recycling (Kontermann, 2011). However,
473 before such technologies can be applied successfully, it is necessary to have a structural
474 understanding of how the active protein element binds to its targets, as we have sought to
475 reveal in the present experiments.

476 In conclusion, we report the rational design of several bispecific selective protein
477 agonists of EPO-R/CD131. These fusion proteins serve as a foundation for future studies of EPO-
478 R/CD131 biology and the development of next-generation cytokine mimetics with improved
479 specificity and reduced off-target effects.

480 # Methods

481 ## DNA construct design and generation

482 The anti-EPO-R scFv sequence was obtained from Moraga et. al (Moraga *et al.*, 2015)
483 (PDB 4y5y) and the anti-CD131 scFv sequence was obtained from Panousis et. al (Panousis *et al.*,
484 2016) (PDB 5dwu). These sequences were codon-optimized and cloned into pSecTag2a. An
485 engineered heterodimeric fragment crystallizable (Fc) domain of mouse IgG2a (H4A, H4B)
486 (Wang *et al.*, 2019) was used in the Fc fusion constructs. The Fc fusions were tagged with His6
487 on one monomer (H4B) to increase the likelihood of purification of only heterodimeric proteins.
488 All protein expression constructs included a secretion signal to enable purification in mammalian
489 cells. Sequences for the spacers of the gRNAs for CD131 KO were designed using the Custom
490 Alt-R™ CRISPR-Cas9 guide RNA tool from IDT against the human CSFR2B locus. Complete
491 sequences of human EPO-R and human CD131 were taken from UniProtKB ID P19235 and
492 UniProtKB ID P32927 respectively and human codon-optimized using Benchling.

493 Plasmids were constructed using multiple fragment isothermal assembly using
494 NEBuilder® HiFi DNA Assembly Master Mix (NEB E2621L) or were ordered as Twist clonal genes.
495 Protein expression plasmids were assembled into pSecTag2a or pOptivec (with added secretion
496 signal from the V-J2-C region of the mouse Ig kappa-chain) to enable protein secretion into the
497 media. All secreted proteins were His6-tagged to enable purification. Overexpression constructs
498 and CRISPR gene editing plasmids were assembled into third-generation lentiviral plasmid
499 backbones for packaging into lentivirus. All plasmids were sequence-verified before use via
500 whole plasmid long-read sequencing (Plasmidsaurus). See Supporting Information for more
501 information on each plasmid (**Supplementary Table 1**), protein sequences (**Supplementary**
502 **Table 6**), full plasmid sequence files and more detailed information on cloning procedures.

503

504

505 ## AlphaFold structural prediction

506 The final predicted structure of the tandem scFv, hEPO-R and hCD131 (**Figure 1E**) was
507 constructed using a combination of AlphaFold 3 (Abramson *et al.*, 2024) and the pyMOL
508 structural align feature. Initially, we generated an AlphaFold 3 prediction of the entire complex
509 (tandem scFv/EPO-R/CD131). However, the resultant predicted structure did not seem
510 biologically plausible. In this model, the transmembrane domain of hEPO-R was sticking
511 perpendicular to the transmembrane domain of hCD131, and the structures did not align well
512 with the solved PDB structures (PDB: 4y5y and 5dwu) of each scFv bound to its respective
513 receptor. Instead, AlphaFold 3 sequences of the EPO-R scFv, hEPO-R and two copies of hCD131
514 were input in AlphaFold 3 to generate a predicted structure. Then, the same was done for the
515 CD131 scFv, hEPO-R and two copies of hCD131. Using the pyMOL align feature, these two
516 structures were combined using the common elements of hEPO-R and 2 hCD131 to align the
517 structures to yield the final structure reported in **Figure 1E**. The measurement feature in PyMOL
518 was used to measure the distance between the termini of the scFvs to design the tandem scFv
519 linker and linker variant proteins (**Figure 1, 4**). See the Supporting Information (**Supplementary**
520 **Figures 1-3**) for a more detailed discussion of model generation and features.
521

522 **Cell culture**

523 HEK293T (ATCC CRL-11268) were obtained from Dr. Rui Tong Quek (Harvard Medical
524 School) and cultured in DMEM (ATCC 30-2002) supplemented with 10% (v/v) fetal bovine serum
525 (FBS; Thermo 10082147). Stable HEK293T overexpression lines expressing either hEPO-R,
526 hCD131 or both hEPO-R and hCD131 were grown in HEK293T complete media as described
527 above supplemented with 10 µg/mL blasticidin (Thermo A1113903) and/or 2.5 µg/mL
528 puromycin (Thermo A1113803). FreeStyle 293-F cell lines (Thermo R79007) were obtained from
529 Dr. Timothy Chang (Harvard Medical School) and cultured in FreeStyle 293 Expression Medium
530 (Thermo 12338026) shaking at 130 rpm in sterile, vented cap Erlenmeyer cell culture shaker
531 flasks (Corning CLS431143-50EA or CLS431145-25EA). UT-7 EPO S1 (UT-7-ES1) were obtained
532 from Dr. R Rogers Yocum and were grown in IMDM (no phenol red) (Thermo 21056023), 10% HI
533 FBS (Thermo 10082147), 1X GlutaMAX™ Supplement (Thermo 35050079), and 20ng/mL human
534 EPO (Peprotech 100-64). UT-7-ES1 with stable CD131 KO were cultured in complete UT-7-ES1

535 media supplemented with 10 µg/mL blasticidin (Thermo A1113903) and 2.5 µg/mL puromycin
536 (Thermo A1113803).

537 HEK293T cell lines were passaged every 3-4 days by gently washing the cell monolayer
538 once with DPBS (Thermo 14190144) followed by lifting with TrypLE (Thermo 12605010) and
539 reseeding at 1/10 – 1/20 dilution (~10% confluence). FreeStyle 293-F cells and UT-7-ES1 cell
540 lines were passaged every 3-4 days or when density reached 1 – 2 million cells/mL and directly
541 reseeded in new flasks at 0.3 – 0.5 million cells/mL. All cell lines were maintained at 37°C and 5%
542 CO_2 in a humidified incubator. A full list of cell lines generated in this work and the
543 corresponding figures they are used in is located in **Supplementary Table 5**.

544

545 **Lentivirus and stable cell line generation**

546 Briefly, stable HEK293T cell lines expressing hEPO-R or hCD131 or both hEPO-R and
547 hCD131 and the UT-7-ES1 CD131 KO line were generated by lentiviral transduction followed by
548 selection with 10 µg/mL blasticidin (Thermo A1113903) and/or 2.5 µg/mL puromycin (Thermo
549 A1113803) depending on the construct. Cells were transduced, incubated for 24-48 hrs and then
550 changed into selection medium. Cell samples were collected once cells recovered to >95%
551 viability to analyze transgene expression or gene KO via SDS-PAGE and western blot or
552 sequencing. See the Supporting Information for more details on the transduction procedure for
553 each of these lines. A full list of cell lines generated in this work and the corresponding figures
554 they are used in is located in **Supplementary Table 5**.

555

556 **SDS-PAGE and Immunostaining**

557 Protein samples or cell lysate were diluted in 4X Laemmli SDS sample buffer (Thermo
558 J60015.AD) and diH_2O water to yield a final 1X Laemmli concentration. Samples were boiled at
559 95°C for 5 minutes to denature proteins and then loaded on 4 to 20% Tris-Glycine gradient gels
560 (Thermo XP04205BOX) submerged in 1X Tris-glycine running buffer (Thermo LC2675). Between
561 100 ng and 10 µg total protein (depending on application) were run alongside 5-10 µL of

562 Novex™ Sharp Pre-stained Protein Standards (Thermo LC5800) for 1 hr at 200V. Gels were rinsed
563 once with diH_2O, stained using SimplyBlue™ SafeStain (Thermo LC6065) following the
564 manufacturer's protocol, and imaged using the Coomassie setting on a ChemiDoc MP (Bio-rad
565 12003154).

566 Gels for immunostaining were instead removed from the cassette, rinsed once with
567 diH_2O in a dish and transferred to a nitrocellulose membrane (Thermo IB23002) according to the
568 manufacturer's protocol using the P0 setting on the iBlot 2 gel transfer device (Invitrogen
569 IB21001). Blots were washed twice while shaking in TBST (TBS (Thermo J60877.K3) + 0.05%
570 Tween-20 (Millipore Sigma P9416-50ML)) and blocked for 1 hr at room temperature or
571 overnight at 4°C while shaking in TBST + 1% BSA (GoldBio A-420-10). Primary antibody was
572 added directly to the blocking solution and incubated shaking for 1 hr at room temperature or
573 overnight at 4°C. Residual primary antibody was removed by washing three times in TBST. Blots
574 were then incubated in secondary antibody diluted in TBST + 1% BSA for 1 hr at room
575 temperature or overnight at 4°C while shaking. Blots were washed three times in TBST to remove
576 unbound secondary antibody, and developed and imaged using SuperSignal West Dura
577 Extended Duration Substrate (Thermo Scientific 34075) and the Chemi setting on a ChemiDoc
578 MP. To quantify western blot signal, band intensities for phospho-STAT5, total STAT5, and the
579 loading control (histone H3) were measured using the ImageLab densitometry software. Bands
580 were background corrected individually by the software, and background-corrected intensities
581 were normalized to the loading control from the same well to account for variations in sample
582 loading. The corrected, normalized phospho-STAT5 signal was then normalized to the
583 corresponding STAT5 signal to account for differences in protein expression levels across
584 samples. Finally, all normalized values were expressed relative to the samples treated with the
585 negative control (PBS), which was set to 1. More detail about the immunostaining protocol and
586 full gel or blot images and analyses are provided in the Supporting Information. Antibody
587 catalog numbers and dilutions are listed in **Supplementary Table 3**.

588

589 **Protein expression and purification**

590 Proteins were expressed transiently in HEK293-F cells using 293-fectin (Thermo
591 12347019) following the manufacturer's protocol. Flasks were incubated for 4-6 days at 37°C, 5%
592 CO2 and shaking at 130 rpm to allow expression and secretion of proteins into the medium.
593 Cells were pelleted and the cell supernatant containing the expressed proteins was isolated. His-
594 tagged proteins were purified from the cleared cell supernatant using His60 Ni Superflow Resin
595 and buffers (Takara 635677) following the manufacturer's protocol. Fractions were taken at each
596 step for later analysis by SDS-PAGE and western blotting using anti-6X His-HRP antibody
597 (Abcam ab1187). Eluted proteins were concentrated and buffer exchanged into endotoxin-free
598 PBS (TekNova P0300) using Amicon Ultra-15 Centrifugal Filters (Millipore-Sigma UFC901008 or
599 UFC901024 depending on protein size) according to the manufacturer's protocol. Protein
600 concentration was assessed using a BCA Protein Assay Kit (Thermo 23227) following the
601 manufacturer's protocol. Purified, concentrated proteins were aliquoted, flash frozen in liquid
602 nitrogen, and stored at -80°C until use. Aliquots were not freeze-thawed more than once to
603 protect protein integrity. A list of all proteins generated in this study is located in
604 **Supplementary Table 4**.

605

606 **Cell lysate generation**

607 3-8 million HEK293T or HEK293T overexpression lines or 4 million UT-7-ES1/UT-7-ES1
608 CD131 KO clone C cells were washed three times using 1X TBS (Thermo J60877.K3) to remove
609 excess cytokine and/or FBS and plated in 60mm dishes or 6-well dishes in serum and cytokine
610 starved media (DMEM only (ATCC 30-2002) for HEK293T lines; IMDM only (Thermo 21056023)
611 for UT-7-ES1). The next day, lysis buffer (1X RIPA (CST 9806S) supplemented with protease and
612 phosphatase inhibitors (Thermo A32961) was prepared and chilled to 4^0C. Wash buffer was
613 prepared and chilled to 4^0C by supplementing 1X TBS with protease and phosphatase inhibitors.
614 Proteins were diluted in media without serum and cytokines to 1 μM, added to cells to yield a
615 final in-plate concentration of 100 nM, and incubated for exactly 15 minutes at 37^0C and 5%
616 CO_2. Cells were washed in wash buffer once and moved to 1.5mL tubes and pelleted by
617 centrifugation for 2 min at 300xg. The cell pellet was resuspended in 200 – 400 μL of lysis buffer

618 and lysed according to the manufacturer's protocol. Protein concentration of the lysates was
619 taken by BCA. Lysates were normalized to the same concentration before analysis by western
620 blotting. See Supporting Information methods for more details.

621

622 **UT-7-ES1 cell proliferation assays**

623 UT-7-ES1 or UT-7-ES1 CD131 KO clone C cell lines were washed three times using TBS to
624 remove residual cytokines and seeded in white, flat-bottom, clear 96-well plates (Millipore
625 Sigma CLS3610) at 9.0 x 10^3 cells per well in 90 µL of growth medium with no growth factors
626 (IMDM + 10% FBS only). The following day, purified proteins were serially diluted 10-fold (10^{-6}
627 M to 10^{-12} M) in growth medium with no growth factors in 96-well plates (Corning 3641) and 10
628 µL of protein dilution or medium was added to the cells. Plates were gently swirled and then
629 incubated at 37°C in 5% CO2 for 72 h. Cell proliferation was determined by Cell Titer Glo
630 (Promega G7572) following the manufacturer's protocol. Luminescence was read on a BioTek
631 Synergy Neo HTS microplate reader using the Luminescence fiber default protocol. Background
632 (media only wells) luminescence was subtracted from each sample and each well's corrected
633 luminescence was divided by the luminescence of untreated cells. Data are reported as
634 proliferation relative to untreated cells and are represented by mean luminescence ± SD of three
635 replicates. EC_{50} and E_{max} were calculated using GraphPad Prism using nonlinear regression
636 (log(agonist) vs. response, variable slope (four parameters).

637

638 **Enzyme-linked immunosorbent assay (Elisa)**

639 Recombinant human EPO-R (RND systems 963-ER) or human CD131 (AcroBio CD1-
640 H5256-100 µg) was diluted to 1 µg/mL in PBS and 50 µL per well was added to coat MaxiSorp
641 96-well ELISA plates (Sigma M9410). Plates were incubated shaking overnight at 4°C and then
642 washed five times in wash buffer (PBS + 0.05% Tween-20 (PBST) (Millipore Sigma P9416-50ML)).
643 Plates were blocked with 200 µL per well of blocking buffer (PBS + 3% BSA (GoldBio A-420-10))
644 for 2 hrs shaking at RT and then washed five times with PBST. His-tagged proteins were serially

645 diluted in PBS, 50 µL per well of each dilution was added, and the plate was incubated for 3 hrs
646 shaking at RT or overnight shaking at 4°C. Plates were washed five times with PBST to remove
647 unbound proteins. Detection antibody (anti-His HRP (Abcam ab1187)) was diluted 1/10,000 in
648 PBS + 3% BSA, and 50 µL was added to each well and incubated at RT shaking for 1hr. Plates
649 were washed five times with PBST to remove unbound antibody. 100 µL of room temperature
650 TMB Substrate solution (Thermo 34028) was added to each well and absorbance was monitored
651 until A_{620} reached >0.8 OD. 2M sulfuric acid was added to stop the reaction, and absorbance was
652 measured at 450 nm. Data are reported as mean A_{450} ± SD of three replicates. EC_{50} and E_{max} were
653 calculated using GraphPad Prism using nonlinear regression (log(agonist) vs. response, variable
654 slope (four parameters).

655

656 **Acknowledgements**

657 The authors thank Professor Timothy Mitchison who provided thoughtful advice on
658 experimental direction. K.E.D. would like to thank Drs. Ethan Jones, Neil Dalvie, Rui Tong Quek,
659 and Kasia Kready for their helpful comments on the manuscript. K.E.D would like to additionally
660 acknowledge the Harvard Systems, Synthetic, and Quantitative Biology PhD program, the
661 Harvard Therapeutics Graduate Program (TGP), and the FujiFilm Fellowship for funding and
662 support.

663

664 **Author Contributions**

665 K.E.D designed the project direction, conceptualized, designed and performed the
666 experiments, made the structural model, and analyzed the data. K.E.D and J.C.W. created the
667 figures and wrote the manuscript. K.E.D., J.C.W, and P.A.S. edited and approve the manuscript.

668

669 **Conflict of interests**

670 The authors declare no competing interests.

Funding

This work was supported by funds from the Department of Defense's Congressionally Directed Medical Research Programs (CDMRP) (TP230429), the Henry Jackson Foundation (award 6615; Air Force Research Laboratory award FA8650-21-2-6250), and the Harvard Brain Science Initiative Seed Grant.

K.E.D., J.C.W., and P.A.S. were also supported by the Harvard Medical School Department of Systems Biology. K.E.D was additionally supported by the Systems, Synthetic and Quantitative Biology PhD program (training award: T32GM135014), the Harvard Therapeutics Graduate Program (TGP) and the FujiFilm Fellowship (2021-2022).

Corresponding Authors

Jeffrey C. Way – Department of Systems Biology, Harvard Medical School, Boston, Massachusetts 02115, United States; Wyss Institute for Biologically Inspired Engineering, Harvard University, Boston, Massachusetts 02115, United States

Email: jeffrey_way@hms.harvard.edu

https://orcid.org/0000-0002-6676-3188

Authors

Kailyn E. Doiron – Department of Systems Biology, Harvard Medical School, Boston, Massachusetts 02115, United States; Wyss Institute for Biologically Inspired Engineering, Harvard University, Boston, Massachusetts 02115, United States

Email: kdoiron@fas.harvard.edu

695 Secondary Email: kailynd126@gmail.com

696 https://orcid.org/0000-0001-5208-788X

697

698 Pamela A. Silver – Department of Systems Biology, Harvard Medical School, Boston,

699 Massachusetts 02115, United States; Wyss Institute for Biologically Inspired Engineering, Harvard

700 University, Boston, Massachusetts 02115, United States

701 Email: pamela_silver@hms.harvard.edu

702 https://orcid.org/0000-0002-7856-4071

703

704 **References**

705 Abramson,J., Adler,J., Dunger,J., *et al.* (2024) *Nature*, **630**, 493–500.

706 Ainavarapu,S.R.K., Brujić,J., Huang,H.H., *et al.* (2006) *Biophys. J.*, **92**, 225.

707 Anagnostou,A., Lee,E.S., Kessimian,N., Levinson,R. and Steiner,M. (1990) *Proc. Natl. Acad. Sci. U. S.*
708 *A.*, **87**, 5978–5982.

709 Boesch,S., Nachbauer,W., Mariotti,C., *et al.* (2014) *Mov. Disord.*, **29**, 935–939.

710 Boesch,S., Sturm,B., Hering,S., Goldenberg,H., Poewe,W. and Scheiber-Mojdehkar,B. (2007) *Ann.*
711 *Neurol.*, **62**, 521–524.

712 Boesch,S., Sturm,B., Hering,S., Scheiber-Mojdehkar,B., Steinkellner,H., Goldenberg,H. and
713 Poewe,W. (2008) *Mov. Disord.*, **23**, 1940–1944.

714 Borges,L.G., Ketchem,R.R., Lim,A.C., Mehlin,C. and Zhou,H. (2008) Erythropoietin receptor
715 agonists.

716 Brines,M. and Cerami,A. (2008) *J. Intern. Med.*, **264**, 405–432.

717 Brines,M. and Cerami,A. (2012) *Mol. Med. Camb. Mass*, **18**, 486–496.

718 Brines,M., Grasso,G., Fiordaliso,F., *et al.* (2004) *Proc. Natl. Acad. Sci.*, **101**, 14907–14912.

719 Brines,M., Patel,N.S.A., Villa,P., *et al.* (2008) *Proc. Natl. Acad. Sci.*, **105**, 10925–10930.

720 Broudy,V.C., Lin,N., Brice,M., Nakamoto,B. and Papayannopoulou,T. (1991) *Blood*, **77**, 2583–2590.

721 Burrill,D.R., Vernet,A., Collins,J.J., Silver,P.A. and Way,J.C. (2016) *Proc. Natl. Acad. Sci.*, **113**, 5245–
722 5250.

723 Carr,P.D., Gustin,S.E., Church,A.P., *et al.* (2001) *Cell*, **104**, 291–300.

724 Casadevall,N., Eckardt,K.U. and Rossert,J.A.A.C.A. (2005) *J. Am. Soc. Nephrol.*, **16**, S67.

725 Caveney,N.A., Rodriguez,G.E., Pollmann,C., *et al.* (2024) *Mol. Cell*, **84**, 1995-2005.e7.

726 Chen,X., Zaro,J. and Shen,W.C. (2013) *Adv. Drug Deliv. Rev.*, **65**, 1357–1369.

727 Cheung Tung Shing,K.S., Broughton,S.E., Nero,T.L., *et al.* (2018) *Sci. Rep.*, **8**, 12457.

728 Chin,H., Nakamura,N., Kamiyama,R., Miyasaka,N., Ihle,J.N. and Miura,O. (1996) *Blood*, **88**, 4415–
729 4425.

730 Cho,B., Yoo,S.J., Kim,S.Y., Lee,C.H., Lee,Y.I., Lee,S.R. and Moon,C. (2022) *Redox Biol.*, **49**, 102223.

731 Ercan,I., Tufekci,K.U., Karaca,E., Genc,S. and Genc,K. (2018) In Donev,R. (ed), *Advances in Protein*
732 *Chemistry and Structural Biology*. Academic Press, pp. 309–357.

733 Gan,Y., Xing,J., Jing,Z., Stetler,R.A., Zhang,F., Luo,Y., Ji,X., Gao,Y. and Cao,G. (2012) *Stroke*, **43**,
734 3071–3077.

735 Ghezzi,P. and Brines,M. (2004) *Cell Death Differ.*, **11 Suppl 1**, S37-44.

736 Grunfeld,J.F., Barhum,Y., Blondheim,N., Rabey,J.M., Melamed,E. and Offen,D. (2007) *Exp. Neurol.*,
737 **204**, 260–263.

738 Hanazono,Y., Sasaki,K., Nitta,H., Yazaki,Y. and Hirai,H. (1995) *Biochem. Biophys. Res. Commun.*,
739 **208**, 1060–1066.

740 Hansen,G., Hercus,T.R., McClure,B.J., *et al.* (2008) *Cell*, **134**, 496–507.

741 He,L., Cohen,E.B., Edwards,A.P.B., *et al.* (2019) *iScience*, **17**, 167–181.

742 Hemani,S., Lane,O., Agarwal,S., Yu,S.P. and Woodbury,A. (2021) *Neurochem. Res.*, **46**, 732–739.

743 Hernández,C.C., Burgos,C.F., Gajardo,A.H., Silva-Grecchi,T., Gavilan,J., Toledo,J.R. and
744 Fuentealba,J. (2017) *Neural Regen. Res.*, **12**, 1381–1389.

745 Jubinsky,P.T., Krijanovski,O.I., Nathan,D.G., Tavernier,J. and Sieff,C.A. (1997) *Blood*, **90**, 1867–1873.

746 Kalantar-Zadeh,K. (2017) *Am. J. Nephrol.*, **45**, 235–247.

747 Kalluru,P.K.R., Bhavanthi,S., Vashist,S., Gopavaram,R.R., Mamilla,M., Sharma,S., Gundoji,C.R. and
748 Goguri,S.R. (2024) *Ann. Med. Surg.*, **86**, 3608–3614.

749 Klingmüller,U., Bergelson,S., Hsiao,J.G. and Lodish,H.F. (1996) *Proc. Natl. Acad. Sci. U. S. A.*, **93**,
750 8324–8328.

751 Komatsu,N., Yamamoto,M., Fujita,H., *et al.* (1993) *Blood*, **82**, 456–464.

752 Kontermann,R.E. (2011) *Curr. Opin. Biotechnol.*, **22**, 868–876.

753 Lauria,G., Bella,E.D., Antonini,G., *et al.* (2015) *J. Neurol. Neurosurg. Psychiatry*, **86**, 879–886.

754 Lee,J., Vernet,A., Gruber,N.G., Kready,K.M., Burrill,D.R., Way,J.C. and Silver,P.A. (2021) *Protein Eng.*
755 *Des. Sel.*, **34**, gzab025.

756 Lee,J., Vernet,A., Redfield,K., Lu,S., Ghiran,I.C., Way,J.C. and Silver,P.A. (2020) *ACS Synth. Biol.*, **9**,
757 191–197.

758 Leist,M., Ghezzi,P., Grasso,G., *et al.* (2004) *Science*, **305**, 239–242.

759 Lim,A.C., Ketchem,R.R., Borges,L., *et al.* (2010) *Biochemistry*, **49**, 3797–3804.

760 Lippi,G., Franchini,M. and Favaloro,E.J. (2010) *Semin. Thromb. Hemost.*, **36**, 537–549.

761 Livnah,O., Stura,E.A., Middleton,S.A., Johnson,D.L., Jolliffe,L.K. and Wilson,I.A. (1999) *Science*, **283**,
762 987–990.

763 Macdougall,IainC., Neubert,P., Coles,GeraldA., Roberts,DavidE., Dharmasena,A.D. and
764 Williams,JohnD. (1989) *The Lancet*, **333**, 425–427.

765 Mariotti,C., Fancellu,R., Caldarazzo,S., *et al.* (2012) *Mov. Disord.*, **27**, 446–449.

766 Masuda,S., Nagao,M., Takahata,K., Konishi,Y., Gallyas,F., Tabira,T. and Sasaki,R. (1993) *J. Biol.*
767 *Chem.*, **268**, 11208–11216.

768 Moraga,I., Wernig,G., Wilmes,S., *et al.* (2015) *Cell*, **160**, 1196–1208.

769 Noh,M.Y., Cho,K.A., Kim,H., Kim,S.M. and Kim,S.H. (2014) *Neurosci. Lett.*, **574**, 53–58.

770 Pankratova,S., Gu,B., Kiryushko,D., Korshunova,I., Køhler,L.B., Rathje,M., Bock,E. and Berezin,V.
771 (2012) *J. Neurochem.*, **121**, 915–923.

772 Panousis,C., Dhagat,U., Edwards,K.M., *et al.* (2016) *mAbs*, **8**, 436–453.

773 Patel,N.S., Nandra,K.K. and Thiemermann,C. (2012) *Crit. Care*, **16**, 229.

774 Philo,J.S., Aoki,K.H., Arakawa,T., Narhi,L.O. and Wen,J. (1996) *Biochemistry*, **35**, 1681–1691.

775 Ponce,L.L., Navarro,J.C., Ahmed,O. and Robertson,C.S. (2013) *Pathophysiology*, **20**, 31–38.

776 Robinson,S., Winer,J.L., Chan,L.A.S., *et al.* (2018) *Front. Neurol.*, **9**.

777 Sautina,L., Sautin,Y., Beem,E., *et al.* (2010) *Blood*, **115**, 896–905.

778 Scott,C.L. and Begley,C.G. (1999) *Int. J. Biochem. Cell Biol.*, **31**, 1011–1015.

779 Sergio,C.M. and Rolando,C.A. (2022) *Exp. Brain Res.*, **240**, 1303–1315.

780 Shimomura,S., Komatsu,N., Frickhofen,N., Anderson,S., Kajigaya,S. and Young,N.S. (1992) *Blood*,
781 **79**, 18–24.

782 Sosnick,T.R., Benjamin,D.C., Novotny,J., Seeger,P.A. and Trewhella,J. (1992) *Biochemistry*, **31**,
783 1779–1786.

784 Syed,R.S., Reid,S.W., Li,C., *et al.* (1998) *Nature*, **395**, 511–516.

785 Tamilvanan,S., Raja,N.L., Sa,B. and Basu,S.K. (2010) *J. Drug Target.*, **18**, 489–498.

786 Wang,F., Tsai,J.C., Davis,J.H., *et al.* (2019) *mAbs*, **12**, 1685350.

787 Watowich,S.S. (1999) *Int. J. Biochem. Cell Biol.*, **31**, 1075–1088.

788 Watowich,S.S. (2011) *J. Investig. Med. Off. Publ. Am. Fed. Clin. Res.*, **59**, 1067–1072.

789 Watowich,S.S., Hilton,D.J. and Lodish,H.F. (1994) *Mol. Cell. Biol.*, **14**, 3535–3549.

790 Watowich,S.S., Liu,K.D., Xie,X., Lai,S.Y., Mikami,A., Longmore,G.D. and Goldsmith,M.A. (1999) *J.*
791 *Biol. Chem.*, **274**, 5415–5421.

792 Witthuhn,B.A., Quelle,F.W., Silvennoinen,O., Yi,T., Tang,B., Miura,O. and Ihle,J.N. (1993) *Cell*, **74**,
793 227–236.

794 Wojchowski,D.M., Gregory,R.C., Miller,C.P., Pandit,A.K. and Pircher,T.J. (1999) *Exp. Cell Res.*, **253**,
795 143–156.

796 Wrighton,N.C., Farrell,F.X., Chang,R., *et al.* (1996) *Science*, **273**, 458–464.

797